

AD-A251 857

2



NASA Contractor Report 189639  
ICASE Report No. 92-17

**DTIC**  
**ELECTE**  
JUN 23 1992  
**S** **C** **D**

# ICASE

**THE MODELING AND CONTROL OF  
ACOUSTIC/STRUCTURE INTERACTION  
PROBLEMS VIA PIEZOCERAMIC ACTUATORS:  
2-D NUMERICAL EXAMPLES**

**H. T. Banks  
R. J. Silcox  
R. C. Smith**

Contract No. NAS1-18605  
April 1992

Institute for Computer Applications in Science and Engineering  
NASA Langley Research Center  
Hampton, Virginia 23665-5225

Operated by the Universities Space Research Association



National Aeronautics and  
Space Administration

Langley Research Center  
Hampton, Virginia 23665-5225

**DISTRIBUTION STATEMENT A**

Approved for public release;  
Distribution Unlimited

**92-16385**



**92 6 22 022**

# THE MODELING AND CONTROL OF ACOUSTIC/STRUCTURE INTERACTION PROBLEMS VIA PIEZOCERAMIC ACTUATORS: 2-D NUMERICAL EXAMPLES <sup>1</sup>

H.T. Banks <sup>2</sup>  
R.J. Silcox <sup>3</sup>  
R.C. Smith <sup>4</sup>



Approved for	<input checked="" type="checkbox"/>
Final	<input type="checkbox"/>
Production	<input type="checkbox"/>
Availability Codes	
Special	
A-1	

## ABSTRACT

The modeling and active control of acoustic pressure in a 2-D cavity with a flexible boundary (a beam) is considered. Control is implemented in the model via piezoceramic patches on the beam which are excited in a manner so as to produce pure bending moments. The incorporation of the feedback control in this manner leads to a system with an unbounded input term. Approximation techniques are discussed and by writing the resulting system as an abstract Cauchy equation, the problem of reducing interior pressure fluctuations can be posed in the context of an LQR time domain state space formulation. Examples illustrating the dynamic behavior of the coupled system as well as demonstrating the viability of the control method on a variety of problems with periodic forcing functions are presented.

<sup>1</sup>The research of H.T.B. was supported in part by the Air Force Office of Scientific Research under grant AFOSR-90-0091 and NASA grant NAG-1-1116. This research was carried out in part while the first author was a visiting scientist at the Institute for Computer Applications in Science and Engineering (ICASE), NASA Langley Research Center, Hampton, VA 23666, which is operated under NASA Contract No. NAS1-18107.

<sup>2</sup>Center for Research in Scientific Computation, North Carolina State University, Raleigh, NC 27695

<sup>3</sup>Acoustics Division, NASA Langley Research Center, Hampton, VA 23665

<sup>4</sup>ICASE, NASA Langley Research Center, Hampton, VA 23665

# 1 Introduction

An important problem in the study of structural acoustics involves the control of noise which is being generated by the vibration of an elastic structure. An example of this is the transmission of sound through an airplane fuselage due to low frequency high amplitude exterior acoustic fields. The need for lighter materials and the development of new fuel efficient turboprop engines has reduced the transmission loss and increased the acoustic and vibration levels thus causing the noise control problem to become a significant impediment to efficiency in recent years.

One means of attempting to decrease the noise levels has been through the use of passive noise control techniques which relied on stiffened structures and material and acoustic damping. In many cases, the increased weight offset the advantages obtained through the use of the new engines and lighter materials.

The active control of noise in this setting has been studied both in a frequency domain setting [11, 12, 13, 16, 17, 19] and from an infinite dimensional state space time domain approach (PDE approach) [1, 4, 5, 10]. Control techniques in these works range from the use of acoustic point sources which generate appropriate secondary pressure waves that optimally *interfere with the offending primary pressure wave to the alteration of structural dynamics through applied point forces and bending moments.* In this latter case, the actuators range from electromagnetic drivers to piezoceramic patches.

In this work, we continue the study of a time domain state space formulation in which the active control is implemented via piezoceramic patches which are bonded to the boundary of the acoustic cavity (a more theoretical background for some of the results in this work can be found in [1]). In this way, we can take advantage of the natural "feedback" loop which is due to the coupling of the structural vibrations and the acoustic fields. Moreover, the piezoceramic patches are light, can be bonded directly to the elastic surface and are relatively cheap to manufacture.

The example we consider consists of an exterior noise source which is separated from an interior chamber by an elastic plate. This plate transmits noise or vibrations from the exterior field to the interior cavity via fluid/structure interactions thus leading to the formulation of a system of partial differential equations consisting of an acoustic wave equation coupled with elasticity equations for the plate. Control is implemented in the example via piezoceramic patches on the plate which are excited in a manner so as to produce pure bending moments which then affect the bending components of the elasticity equations. Because the incorporation of the feedback control is through actuators covering only sections of the boundary, the resulting system contains an unbounded input term. Experiments are being designed and carried out at NASA Langley Research Center in which the interior cavity is taken to be cylindrical with a circular elastic plate and sectorial patches.

As a first step toward developing an effective linear quadratic regulator (LQR) state space control methodology for near field acoustic problems of this type, it is useful to consider a simplified but typical model consisting of a 2-D interior cavity with an elastic beam at one end (see Figure 1). Here  $\mathcal{F}$  represents a perturbing force on the beam due to an exterior noise source. This in turn causes fluctuations in the interior acoustic pressure field and hence unwanted noise. The goal in the control problem is to optimally reduce the interior pressure deviations by effecting a force distribution on the beam that decouples the cavity acoustic response from the beam response or primary excitation.

In Section 2, a model set of differential equations for the problem is given and the mathematical framework needed to pose the control system in variational form is discussed. The finite dimensional approximation of the control problem is presented in Section 3. After discussing suitable choices for the bases, the discrete system is formulated as a finite dimensional Cauchy equation. With the problem in this format, the control gains can be obtained in terms of the solution of the algebraic Riccati equation. Section 4 contains examples demonstrating both modeling and control results. The first example illustrates the dynamic behavior of the coupled system with the next three examples demonstrating the viability of the control method on a variety of problems with periodic forcing functions.

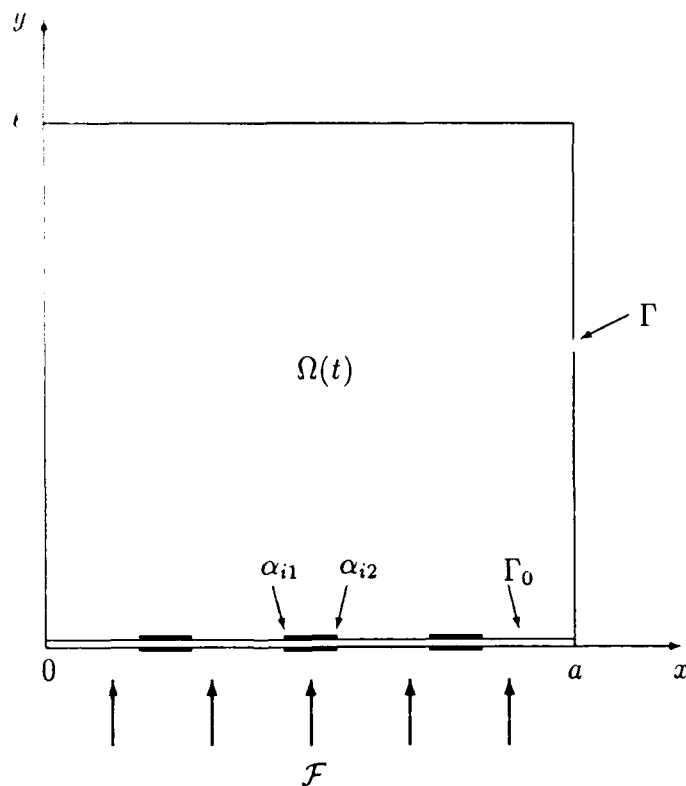


**Figure 1.** Acoustic chamber with piezoceramic patches.

## 2 Mathematical Model

When describing the interaction between the acoustic wave motion in the fluid and the vibration of the structure, both the fluid velocity,  $\vec{v}$ , and the acoustic pressure,  $p$ , (the deviation from the mean pressure at equilibrium) are physically significant. In order to simplify the resulting equations, it is useful to introduce a velocity potential  $\phi$  which is a complex-valued function from which the characteristic values  $\vec{v}$  and  $p$  can be calculated by means of simple differential equations. The velocity potential is determined by the relation  $\vec{v}(t, x, y) = -\nabla\phi(t, x, y)$  and the pressure is related to this velocity potential by  $p(t, x, y) = \rho_f\phi_t(t, x, y)$  where  $\rho_f$  is the equilibrium density of the fluid.

For acoustic waves with small amplitude, both the potential and the pressure satisfy the undamped wave equation with uniform speed of sound  $c$  in the fluid [14, 15]; hence

$$\phi_{tt} = c^2\Delta\phi \quad (x, y) \in \Omega(t), t > 0.$$

The boundaries on three sides of the variable cavity  $\Omega(t)$  are taken to be "hard" walls thus leading to the zero normal velocity boundary conditions

$$\nabla\phi \cdot \hat{n} = 0 \quad (x, y) \in \Gamma, t > 0$$

where  $\hat{n}$  is the outer normal. It is assumed that the perturbable boundary consists of an impenetrable fixed-end Euler-Bernoulli beam with Kelvin-Voigt damping. If  $w(t, x)$  is used to denote the transverse displacement of the beam with linear mass density  $\rho_b$ , the equations of motion are

$$\begin{aligned} \rho_b w_{tt} + \frac{\partial^2}{\partial x^2} M(t, x) &= -\rho_f \phi_t(t, x, w(t, x)) + f(t, x) & 0 < x < a, \\ & & t > 0, \\ w(t, 0) = \frac{\partial w}{\partial x}(t, 0) = w(t, a) = \frac{\partial w}{\partial x}(t, a) &= 0 & t > 0, \end{aligned} \quad (2.1)$$

where  $M(t, x)$  is the internal moment and  $f$  is the external applied force due to pressure from an exterior noise field. For an uncontrolled beam with Kelvin-Voigt damping, the moment contains both strain and strain rate components and is given by

$$M(t, x) = EI \frac{\partial^2 w}{\partial x^2} + c_D I \frac{\partial^3 w}{\partial x^2 \partial t}.$$

The final coupling equation is the continuity of velocity condition

$$w_t(t, x) = \nabla\phi(t, x, w(t, x)) \cdot \hat{n}, \quad 0 < x < a, t > 0 \quad (2.2)$$

which results from the assumption that the beam is impenetrable to fluid. Under an assumption of small displacements ( $w(t, x) = \hat{w}(t, x) + \delta$  where  $\hat{w} \equiv 0$ ) which is inherent in the Euler-Bernoulli formulation, the beam equation in (2.1) can be approximated by

$$\rho_b w_{tt} + \frac{\partial^2}{\partial x^2} M(t, x) = -\rho_f [\phi_t(t, x, 0) + \phi_{ty}(t, x, 0)w] + f(t, x)$$

while (2.2) can be approximated by

$$w_t(t, x) = \nabla\phi(t, x, 0) \cdot \hat{n} + (\nabla\phi_y(t, x, 0)w) \cdot \hat{n} .$$

To first order, these last two equations can be approximated by dropping the higher order terms  $-\rho_f\phi_{ty}(t, x, 0)w$  and  $(\nabla\phi_y(t, x, 0)w) \cdot \hat{n}$ . Then upon approximating the domain  $\Omega(t)$  by the fixed domain  $\Omega \equiv [0, a] \times [0, \ell]$ , we obtain the approximate uncontrolled model

$$\phi_{tt} = c^2\Delta\phi \quad (x, y) \in \Omega, t > 0 ,$$

$$\nabla\phi \cdot \hat{n} = 0 \quad (x, y) \in \Gamma, t > 0 ,$$

$$\frac{\partial\phi}{\partial y}(t, x, 0) = -w_t(t, x) \quad 0 < x < a, t > 0 ,$$

$$\rho_b w_{tt} + \frac{\partial^2}{\partial x^2} \left( EI \frac{\partial^2 w}{\partial x^2} + c_D I \frac{\partial^3 w}{\partial x^2 \partial t} \right) = -\rho_f \phi_t(t, x, 0) + f(t, x) \quad \begin{array}{l} 0 < x < a , \\ t > 0 , \end{array} \quad (2.3)$$

$$w(t, 0) = \frac{\partial w}{\partial x}(t, 0) = w(t, a) = \frac{\partial w}{\partial x}(t, a) = 0 \quad t > 0 ,$$

$$\phi(0, x, y) = \phi_0(x, y) \quad , \quad w(0, x) = w_0(x)$$

$$\phi_t(0, x, y) = \phi_1(x, y) \quad , \quad w_t(0, x) = w_1(x) .$$

For control of structural vibrations and the acoustic pressure field in this model,  $s$  piezoceramic patches are attached to the beam as shown in Figure 1. These patches are excited in a manner so as to produce pure bending moments ([6, 7, 9]) (see Figure 2). If  $H$  is used to denote the Heaviside function, the model for the controlled beam can be written as

$$\begin{aligned} \rho_b w_{tt} + \frac{\partial^2}{\partial x^2} \left( EI \frac{\partial^2 w}{\partial x^2} + c_D I \frac{\partial^3 w}{\partial x^2 \partial t} \right) + \rho_f \phi_t(t, x, 0) \\ = \frac{\partial^2}{\partial x^2} \left( EI \frac{K^B d_{31}}{\mathcal{T}} \sum_{i=1}^s u_i(t) [H(x - \alpha_{i1}) - H(x - \alpha_{i2})] \right) + f(t, x) . \end{aligned} \quad (2.4)$$

Here  $u_i(t)$  is the voltage applied to the  $i^{\text{th}}$  patch,  $K^B$  is a parameter which depends on the geometry and piezoceramic material properties,  $\mathcal{T}$  is the patch thickness and  $d_{31}$  is the piezoelectric strain constant (see [6, 7]). It should be noted that the incorporation of (2.4) into (2.3) leads to a system with an unbounded input term since it involves the second derivative of the Heaviside function.

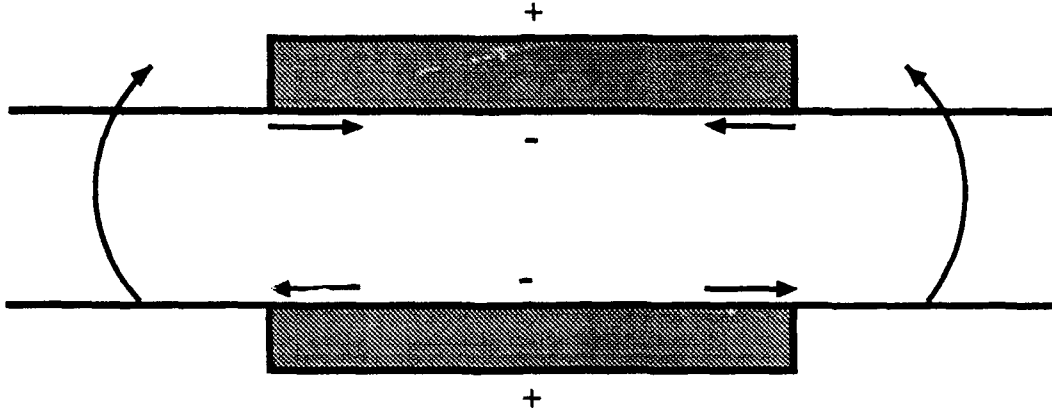


Figure 2. Piezoceramic patch excitation.

In order to pose this problem in a manner which is conducive to approximation and control, the state is taken to be  $z = (\phi, w)$  in the state space  $H = \bar{L}^2(\Omega) \times L^2(\Gamma_0)$ . Here  $\bar{L}^2(\Omega)$  is the quotient space of  $L^2$  over the constant functions. The use of the quotient space results from the fact that the potentials are determined only up to a constant.

To provide a class of functions which are considered when defining a variational form of the problem, we also define the Hilbert space  $V = \bar{H}^1(\Omega) \times H_0^2(\Gamma_0)$  where  $\bar{H}^1(\Omega)$  is the quotient space of  $H^1$  over the constant functions and  $H_0^2(\Gamma_0)$  is given by  $H_0^2(\Gamma_0) = \{\psi \in H^2(\Gamma_0) : \psi(x) = \psi'(x) = 0 \text{ at } x = 0, a\}$ .

A complete discussion concerning the first and second order weak or variational forms of the control system is given in [1]. For our purposes here, it suffices to note that from (2.3) and (2.4), it follows that the second-order system in variational form is given by

$$\begin{aligned}
 & \int_{\Omega} \frac{\rho_f}{c^2} \phi_{tt} \xi d\omega + \int_{\Gamma_0} \rho_b w_{tt} \eta d\gamma \\
 & + \int_{\Omega} \rho_f \nabla \phi \cdot \nabla \xi d\omega + \int_{\Gamma_0} EID^2 w D^2 \eta d\gamma \\
 & + \int_{\Gamma_0} \{c_D ID^2 w_t D^2 \eta + \rho_f (\phi_t \eta - w_t \xi)\} d\gamma \quad (2.5) \\
 & = \int_{\Gamma_0} EI \frac{K^B d_{31}}{T} \sum_{i=1}^s u_i(t) (H_{i1} - H_{i2}) D^2 \eta d\gamma \\
 & + \int_{\Gamma_0} f \eta d\gamma
 \end{aligned}$$

for all  $(\xi, \eta)$  in  $V$ . In order to simplify the above expression, we have adapted the notation  $H_{ij}(x) \equiv H(x - \alpha_{ij})$ ,  $i = 1, \dots, s$ ,  $j = 1, 2$ . The system can be written in first-order form by defining the product spaces  $\mathcal{V} = V \times V$  and  $\mathcal{H} = V \times H$  and taking the state to be  $\mathcal{Z} = (\phi, w, \dot{\phi}, \dot{w})$ . Note that the state now contains a multiple of the pressure since  $p = \rho_f \dot{\phi}$ .

The first-order variational form is

$$\begin{aligned}
& \int_{\Omega} \frac{\rho_f}{c^2} (\dot{\phi})_t \xi d\omega + \int_{\Gamma_0} \rho_b (\dot{w})_t \eta d\gamma \\
& + \int_{\Omega} \rho_f \nabla \phi \cdot \nabla \xi d\omega + \int_{\Gamma_0} EI D^2 w D^2 \eta d\gamma \\
& + \int_{\Gamma_0} \{c_D I D^2 \dot{w} D^2 \eta + \rho_f (\dot{\phi} \eta - \dot{w} \xi)\} d\gamma \\
& = \int_{\Gamma_0} EI \frac{K^B d_{31}}{T} \sum_{i=1}^s u_i(t) (H_{i1} - H_{i2}) D^2 \eta d\gamma \\
& + \int_{\Gamma_0} f \eta d\gamma
\end{aligned} \tag{2.6}$$

for all  $(\xi, \eta)$  in  $V$ . Again, a more complete discussion concerning the formulation of the first-order system in weak form is given in [1].

### 3 Finite Dimensional Approximation and Control

The problem (2.6) is now in a form which is amenable both to approximation and control. As shown in [1], the infinite dimensional system can be formally written as an abstract Cauchy equation, and periodic infinite dimensional control results similar to those found in [8] can be applied (see also [2, 3]). Approximate feedback gains (and hence controlling voltages) can be obtained by using a standard Galerkin approach in which one chooses a sequence of finite dimensional subspaces  $\mathcal{H}^N \subset \mathcal{H}$  with projections  $\mathcal{P}^N : \mathcal{H} \rightarrow \mathcal{H}^N$ . In order to guarantee the convergence of the approximate gains to those of the infinite dimensional system, it is sufficient to impose various conditions on the original and approximation systems. These hypotheses include convergence requirements for the uncontrolled problem as well as the requirement that the approximation systems preserve stabilizability and detectability margins uniformly.

Cubic splines are used as a basis for the beam since they satisfy the smoothness requirements as well as being easily implemented when adapting to the fixed-end boundary conditions and patch discretizations. Letting  $\{B_i^n\}_{i=1}^{n-1}$  denote the cubic splines which have been modified to satisfy the boundary conditions (see [1] for details), the corresponding  $n-1$  dimensional approximating subspace is given by  $H_b^n = \text{span} \{B_i^n\}_{i=1}^{n-1}$  and the approximate beam solution is taken to be

$$w^N(t, x) = \sum_{i=1}^{n-1} w_i^N(t) B_i^n(x).$$

The 2-D cavity basis is taken to be  $\{B_i^m\}_{i=1}^m$  where  $B_i^m(x, y)$  is the tensor product of 1-D Legendre polynomials which have been scaled by transformation to the  $x$  and  $y$  intervals  $[0, a]$  and  $[0, \ell]$ , respectively. The total number of cavity basis functions,  $m = (m_x + 1) \cdot (m_y + 1) - 1$ , reflects the deletion of the constant function so as to guarantee that the set of functions is

suitable as a basis for the quotient space. No boundary modifications are needed for the Legendre basis since natural boundary conditions occur on all sides of the cavity. The  $m$  dimensional approximating subspace is then taken to be  $H_c^m = \text{span} \{B_i^m\}_{i=1}^m$  and the approximate cavity solution is given by

$$\phi^N(t, x, y) = \sum_{i=1}^m \phi_i^N(t) B_i^m(x, y).$$

The approximating state space is then taken to be  $H^N = H_c^m \times H_b^n$  where  $N = m + n - 1$ , and the product space for the first order system is  $\mathcal{H}^N = H^N \times H^N$ . As shown in [1], the restriction of the infinite dimensional system (2.5) to  $\mathcal{H}^N \times \mathcal{H}^N$  yields

$$\begin{aligned} M^N \dot{y}^N(t) &= \tilde{A}^N y^N(t) + \tilde{B}^N u(t) + \tilde{F}^N(t) \\ M^N y^N(0) &= \tilde{y}_0^N \end{aligned}$$

or equivalently the finite dimensional Cauchy equation

$$\begin{aligned} \dot{y}^N(t) &= A^N y^N(t) + B^N u(t) + F^N(t) \\ y^N(0) &= y_0^N. \end{aligned} \tag{3.1}$$

Explicit descriptions of the mass and stiffness matrices  $M^N$  and  $\tilde{A}^N$  as well as detailed definitions of the control matrix  $\tilde{B}^N$  and the force vector  $\tilde{F}^N(t)$  can be found in [1]. The  $2N \times 1$  vector  $y^N(t) = (\phi_1^N(t), \dots, \phi_m^N(t), w_1^N(t), \dots, w_{n-1}^N(t), \dot{\phi}_1^N(t), \dots, \dot{\phi}_m^N(t), \dot{w}_1^N(t), \dots, \dot{w}_{n-1}^N(t))^T$  contains the approximate state coefficients while  $u(t) = (u_1(t), \dots, u_s(t))^T$  contains the  $s$  control variables. The periodic finite dimensional control problem is then to find  $u \in L^2(0, \tau)$  which minimizes

$$J^N(u) = \frac{1}{2} \int_0^\tau \{ \langle Q^N y^N(t), y^N(t) \rangle_{\mathbf{R}^N} + \langle Ru(t), u(t) \rangle_{\mathbf{R}^s} \} dt, \quad N = m + n - 1$$

where  $y^N$  solves (3.1),  $\tau$  is the period,  $R$  is an  $s \times s$  diagonal matrix and  $r_{ii} > 0, i = 1, \dots, s$  is the weight on the controlling voltage into the  $i^{\text{th}}$  patch.

The nonnegative definite matrix  $Q^N$  can be chosen so as to emphasize the minimization of particular state variables as well as to create windows that can be used to decrease state variations of certain frequencies. From energy considerations as discussed in [1], an appropriate choice for  $Q^N$  in this case is

$$Q^N = M^N \mathcal{D}$$

where  $M^N$  again is the mass matrix, and the diagonal matrix  $\mathcal{D}$  is given by

$$\mathcal{D} = \text{diag} [d_1 I^m, d_2 I^{n-1}, d_3 I^m, d_4 I^{n-1}] .$$

Here  $I^k, k = m, n - 1$ , denotes a  $k \times k$  identity and the parameters  $d_i$  are chosen to enhance stability and performance of the feedback.

The optimal control is then given by

$$u^N(t) = R^{-1} (B^N)^T [r^N(t) - \Pi^N y^N(t)]$$

where  $\Pi^N$  is the solution to the algebraic Riccati equation

$$(A^N)^T \Pi^N + \Pi^N A^N - \Pi^N B^N R^{-1} (B^N)^T \Pi^N + Q^N = 0 . \quad (3.2)$$

For the regulator problem with periodic forcing function  $F^N(t)$ ,  $r^N(t)$  solves the linear differential equation

$$\begin{aligned} \dot{r}^N(t) &= - \left[ A^N - B^N R^{-1} (B^N)^T \Pi^N \right]^T r^N(t) + \Pi^N F^N(t) \\ r^N(0) &= r^N(\tau) \end{aligned} \quad (3.3)$$

while the optimal trajectory is the solution to the linear differential equation

$$\begin{aligned} \dot{y}^N(t) &= \left[ A^N - B^N R^{-1} (B^N)^T \Pi^N \right] y^N(t) + B^N R^{-1} (B^N)^T r^N(t) + F^N(t) \\ y^N(0) &= y^N(\tau) . \end{aligned} \quad (3.4)$$

## 4 Numerical Results

The general problem under consideration in the following examples is

$$\begin{aligned} \phi_{tt} &= c^2 \Delta \phi \quad (x, y) \in \Omega , t > 0 , \\ \nabla \phi \cdot \hat{n} &= 0 \quad (x, y) \in \Gamma , t > 0 , \\ \frac{\partial \phi}{\partial y}(t, x, 0) &= -w_t(t, x) \quad 0 < x < .6 , t > 0 , \\ \rho_b w_{tt} + \frac{\partial^2}{\partial x^2} \left( EI \frac{\partial^2 w}{\partial x^2} + c_{DI} \frac{\partial^3 w}{\partial x^2 \partial t} \right) & \\ &= \frac{\partial^2}{\partial x^2} \left( EI \frac{K^B d_{31}}{\mathcal{T}} u(t) [H(x - \alpha_{11}) - H(x - \alpha_{12})] \right) \\ &- \rho_f \phi_t(t, x, 0) + f(t, x) \quad 0 < x < .6 , t > 0 , \\ w(t, 0) = \frac{\partial w}{\partial x}(t, 0) = w(t, .6) = \frac{\partial w}{\partial x}(t, .6) &= 0 \quad t > 0 , \\ \phi(0, x, y) = \phi_t(0, x, y) = w(0, x) = w_t(0, x) &= 0 . \end{aligned} \quad (4.1)$$

The parameter choices  $a = .6 \text{ m}$ ,  $\ell = 1 \text{ m}$ ,  $\rho_f = 1.21 \text{ kg/m}^3$ ,  $c^2 = 117649 \text{ m}^2/\text{sec}^2$ ,  $\rho_b = 1.35 \text{ kg/m}$ ,  $EI = 73.96 \text{ Nm}^2$ ,  $c_{DI} = .001 \text{ kg m}^3/\text{sec}$ ,  $K^B = 82.9629$ ,  $\mathcal{T} = .0005 \text{ m}$ , and  $d_{31} = 1.9 \times 10^{-10} \text{ m/V}$ , are physically reasonable for a .6 m by 1 m cavity in which the bounding end beam has a centered piezoceramic patch. The beam is assumed to have width and thickness .1 m and .005 m, respectively. For an undamped fixed-fixed beam with the above dimensions and density, the natural frequencies of the first three modes are

$$\begin{aligned} f_1 &= 73.2 \text{ hertz} , \\ f_2 &= 201.8 \text{ hertz} , \\ f_3 &= 395.6 \text{ hertz} , \end{aligned}$$

respectively. Likewise, for pressure oscillations in a cavity of this size, the natural frequencies of the modes are given by  $\omega = \frac{mc}{2L}$ ,  $m = 1, 2, \dots$ , where  $L = \ell = 1$  in the  $y$ -direction and  $L = a = .6$  in the  $x$ -direction. Note that both sets of frequencies are for the uncoupled systems.

## 4.1 System Dynamics

In this example, we determine the behavior of the uncontrolled coupled system when the forcing function  $f$  is taken to be an impulse at the center of the beam; that is,

$$f(t, x) = \delta(x - .3)\delta(t).$$

From the response, the natural frequencies and dynamic behavior of the system can be determined and compared to those of the uncoupled beam and cavity. Note that from the definitions of the component matrices and vectors, it follows immediately that the right hand side vector  $\dot{F}_2^N(t)$  has elements given by

$$\begin{aligned} [\dot{F}_2^N(t)] &= \int_{\Gamma_0} f B_p^n d\gamma \\ &= B_p^n(.3)\delta(t) \end{aligned}$$

where  $B_p^n$  denotes a modified cubic spline basis function. Thus  $\dot{F}_2^N(t)$  is simply given by  $\dot{F}_2^N(t) = [0, \dots, 0, 1, 4, 1, 0, \dots, 0]^T \delta(t)$ . Note that this contribution is included only at time  $T = 0$  after which the system is allowed to run unforced through time  $T = 20/75$ . This temporal interval is sufficient for demonstrating the dynamic behavior of the system.

The beam and pressure responses obtained with  $m_x = m_y = 12$  and  $n = 16$  basis functions at the points  $X = .3$  and  $(X, Y) = (.3, .1)$  are plotted in Figure 3 with corresponding frequency plots in Figure 4. From Figure 3 it can be seen that due to the damping in the beam, both the beam and pressure oscillations are gradually decreasing in magnitude as the system is allowed to run unforced. The frequency plots in Figure 4 indicate the presence of several natural frequencies for the coupled system. Although one would expect these frequencies to correspond in some manner to the individual natural frequencies of the beam and cavity, one must also note that the system (4.1) involves not only coupling between the cavity and beam equations but also includes damping in the beam. Indeed, the system responses at 65.9 and 387.8 hertz are slightly lower in frequency than the natural frequencies of the first two symmetric modes of the undamped beam which have values of 73.2 and 395.6 hertz. The remaining resonant peaks are due to pressure oscillations in the cavity. The responses at 181.3 and 343.9 hertz are slightly higher than the values of 171.5 and 343 hertz which are the first two natural frequencies in the  $y$ -direction for pressure oscillations in a cavity of this size. A response at 519 hertz corresponding to the third harmonic (514 hertz) in the  $y$ -direction can be seen if one considers data taken over the much shorter time interval,  $[0, 3/75]$ . This response has very low energy however, and has died away long before  $T = 20/75$ . As seen in Figures 11 and 18 of Sections 4.3 and 4.4, system oscillations at this frequency are more pronounced when produced by a forcing function which is acting over a longer temporal interval.

The system response at 572.4 hertz corresponds to the uncoupled cavity frequency of 571.7 hertz for the second  $x$  mode. Because the excitation is symmetric in  $x$ , one does not see a response corresponding to the nonsymmetric first  $x$  mode having the frequency 285.8 hertz. It is more difficult to determine correspondences between higher frequency system modes (600 hertz and above) and those of the uncoupled beam and cavity. This may in part be due to higher frequency effects of coupling and damping. Finally, it should be noted that the mode shapes for the coupled system as well as the natural frequencies are slightly different than those of the component beam and cavity; hence care must be taken when describing the dynamics of the coupled system in terms of the properties of the undamped and uncoupled beam and cavity.

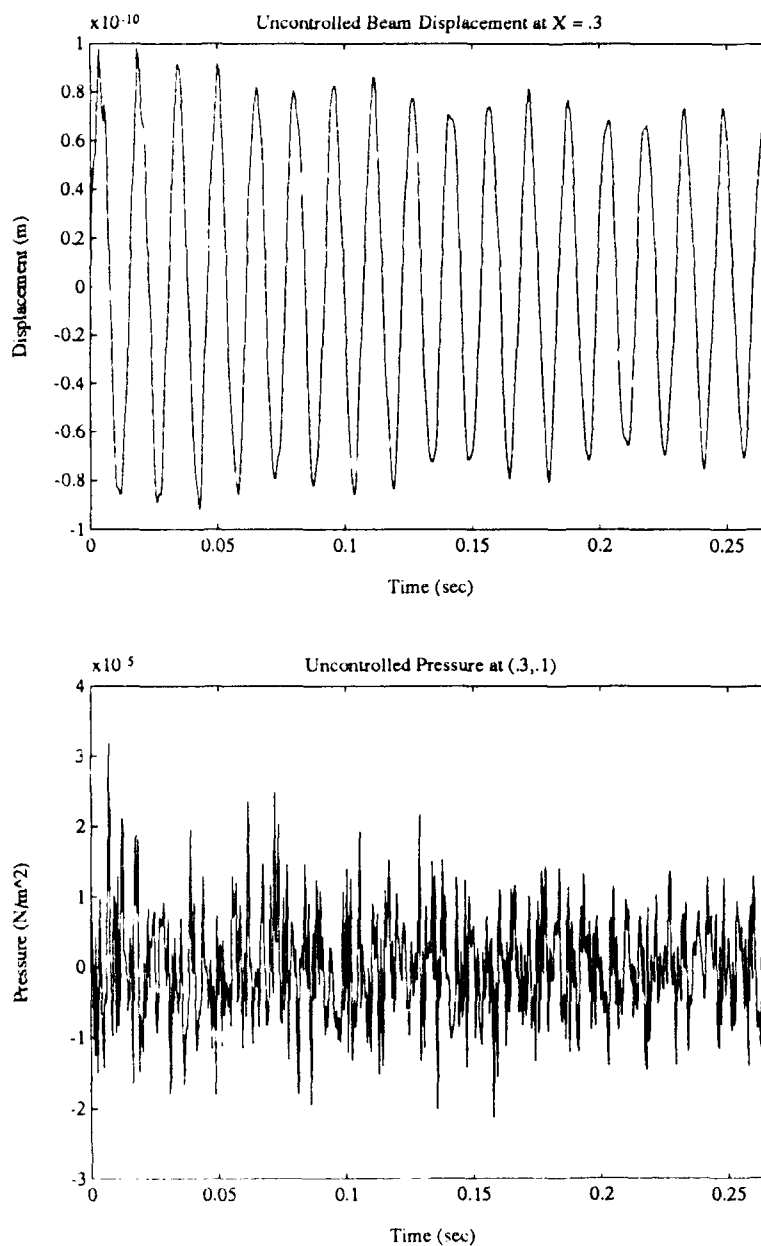


**Figure 3.** The beam and pressure responses to a centered impact.

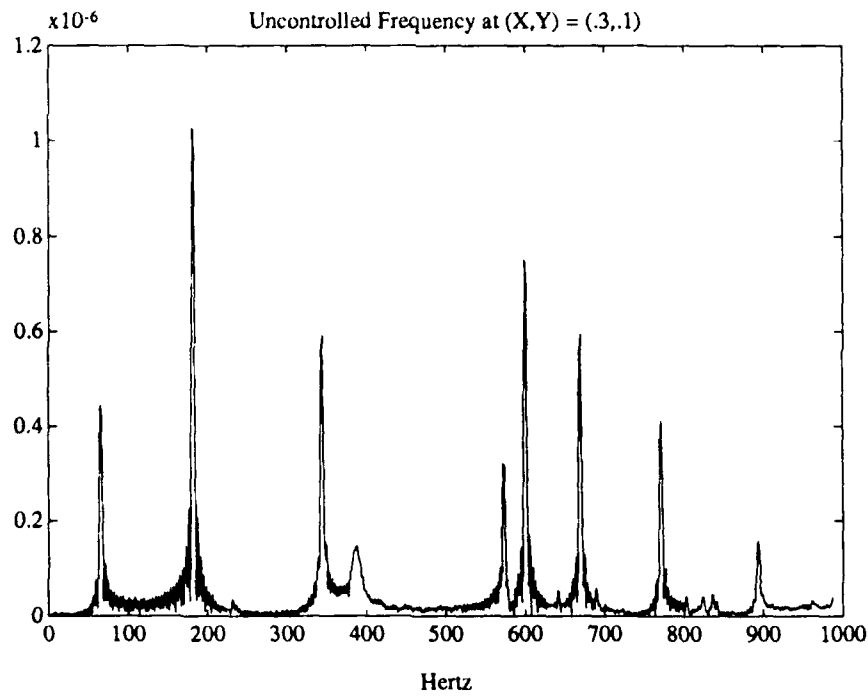
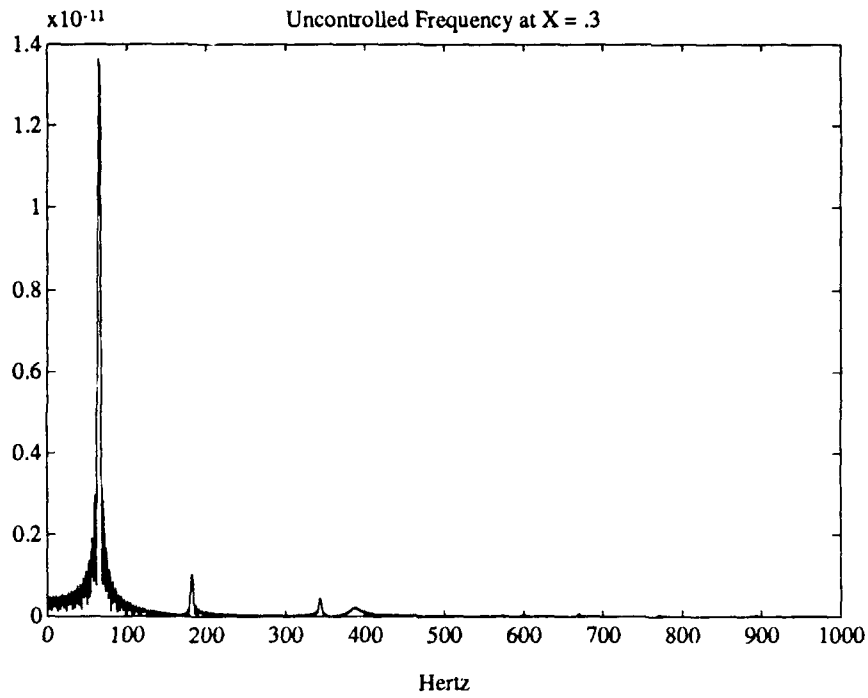


**Figure 4.** The beam and pressure frequency responses to a centered impact.

## 4.2 Resonant Excitation

In the following examples, the effects of feedback control on the system (4.1) for various forcing functions are described. The forcing function in this example is

$$f(t, x) = 2.04 \sin(150\pi t)$$

which corresponds to a frequency of 75 hertz and hence is close to the natural frequency of the first system mode which is 65.9 hertz (see Section 4.1). This models a periodic exterior plane wave with a root mean square (rms) sound pressure level of 117 dB.

Control was implemented via a single centered piezoceramic patch covering 1/6 of the beam length (see Figure 5). The quadratic cost functional parameters were taken to be  $d_1 = d_2 = d_4 = 1$ ,  $d_3 = 10^4$  and  $R = 10^{-6}$  with  $d_3$  of much larger magnitude than  $d_1, d_2$  or  $d_4$  to emphasize the penalization of large pressure variations. When running the uncontrolled problem, the beam and pressure oscillations could be fully resolved with the choices  $m_x = m_y = 4$  and  $n = 8$ . In the control problem however, a larger number of basis functions was needed to fully resolve the early transient behavior and the results which follow were obtained with the choices  $m_x = m_y = 8$  and  $n = 12$ . Note that this results in a total of 80 cavity and 11 beam basis functions.

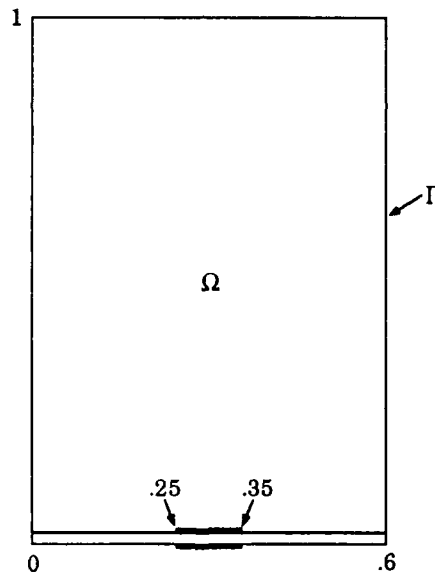


**Figure 5.** Acoustic chamber with one centered 1/6 length piezoceramic patch.

In order to solve for the optimal control and trajectory, it is necessary to solve not only the algebraic Riccati equation (3.2), but also the trajectory equation (3.4) and the tracking equation (3.3). The gains from the Riccati equation were calculated via Potter's method (see [18]). Because numerical evidence indicated that the unconstrained solutions to the trajectory and tracking equations were roughly periodic with period  $\tau = 1/75$ , the problems were solved as initial value problems with starting values  $y(0) = 0$  and  $r(10/75) = 0$  rather than as free boundary value problems. The choice for initial state is physically reasonable

while the choice to integrate backwards in time in (3.3) is made to reduce numerical instability when solving the ODE system for  $r^N(t)$ .

The uncontrolled and controlled approximate beam displacements and acoustic pressures ( $p^N = \rho_f \phi_i^N$ ) at the points  $X = .3$  and  $(X, Y) = (.3, .1)$  are plotted in Figure 6 for the time interval  $[0, 10/75]$ . The uncontrolled solutions exhibit a beat phenomenon which results from the fact that the frequency of the forcing function is slightly greater than the natural frequency of the first system mode. From this data, it can be determined that the uncontrolled rms pressure at the point  $(X, Y) = (.3, .1)$  is  $p_{rms} = 1.0957 \text{ N/m}^2$ . This yields an uncontrolled interior sound pressure level of 94.6 dB. After a transient interval, the controlled solutions are periodic and are maintained at a level which is approximately 10% of that found in the uncontrolled case. The controlled rms pressure is  $p_{rms} = .125 \text{ N/m}^2$  and the controlled interior sound pressure level is maintained at 75.8 dB which is a 18.8 dB reduction.

The frequencies of the uncontrolled and controlled beam displacements and cavity pressures are plotted in Figure 7 (note the differing scales in the plots). The uncontrolled beam plot shows the presence of the forcing frequency as well as the slightly lower natural system frequency while the uncontrolled cavity plot also shows a slight system response at 180 hertz. The controlled response in both cases shows only the presence of the forcing frequency.

To further illustrate the state reduction with feedback control, the uncontrolled and controlled acoustic pressures at the times  $T = 1/75, 2/75, 6/75$  and  $10/75$  are plotted in Figure 9. These are shown as surface plots illustrating the pressure amplitude distribution throughout the acoustic cavity. These results are representative of those found throughout the time interval  $[0, 10/75]$  and in conjunction with Figure 6, demonstrate that the pressure and beam displacement are uniformly reduced and maintained at a very low level of magnitude in spite of the periodic forcing function.

The controlling voltage  $u(t)$  is plotted in Figure 8. As expected, it is periodic with period  $1/75$ . It should be noted that the magnitude of  $u(t)$  remains less than 60V which is a physically reasonable voltage to put into the piezoceramic patches.

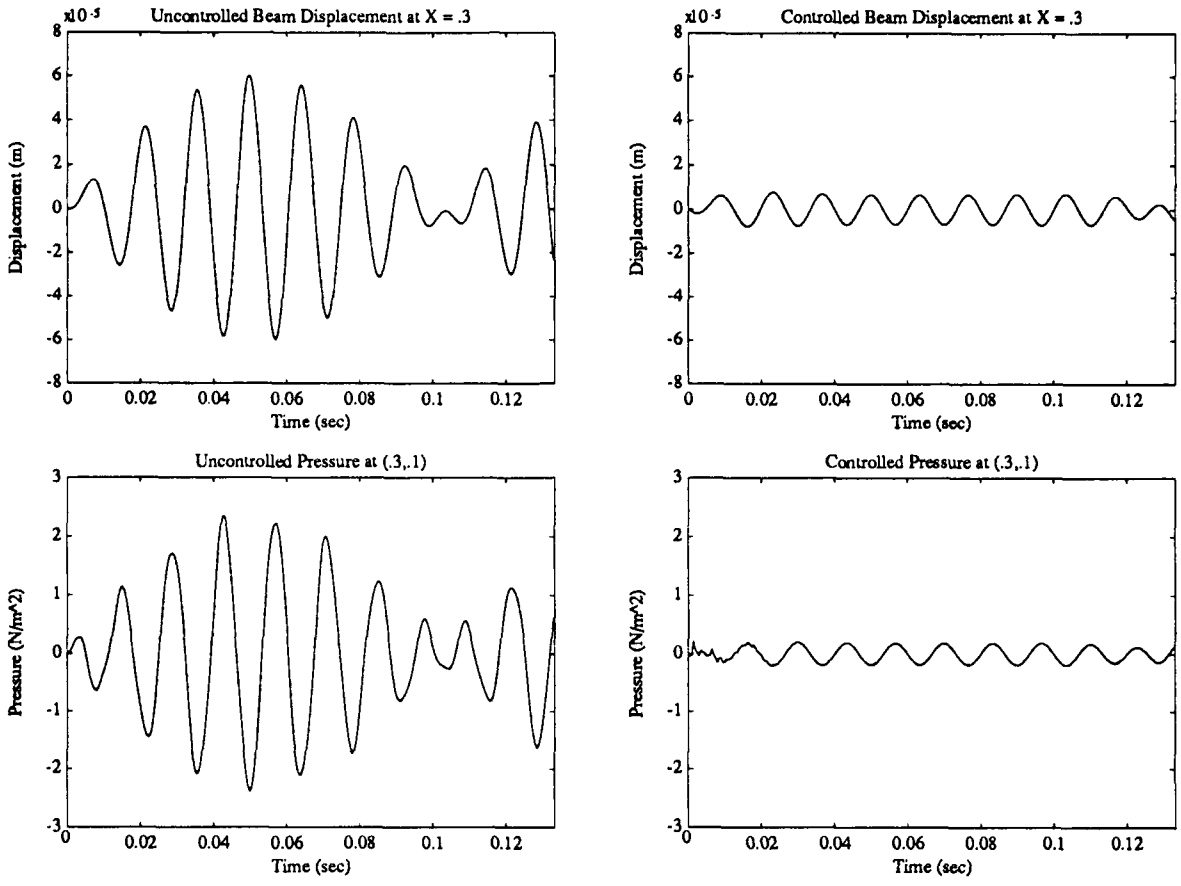


**Figure 6.** Uncontrolled and controlled beam displacements and pressures at the points  $X = .3$  and  $(X, Y) = (.3, .1)$  throughout the time interval  $[0, 10/75]$ .

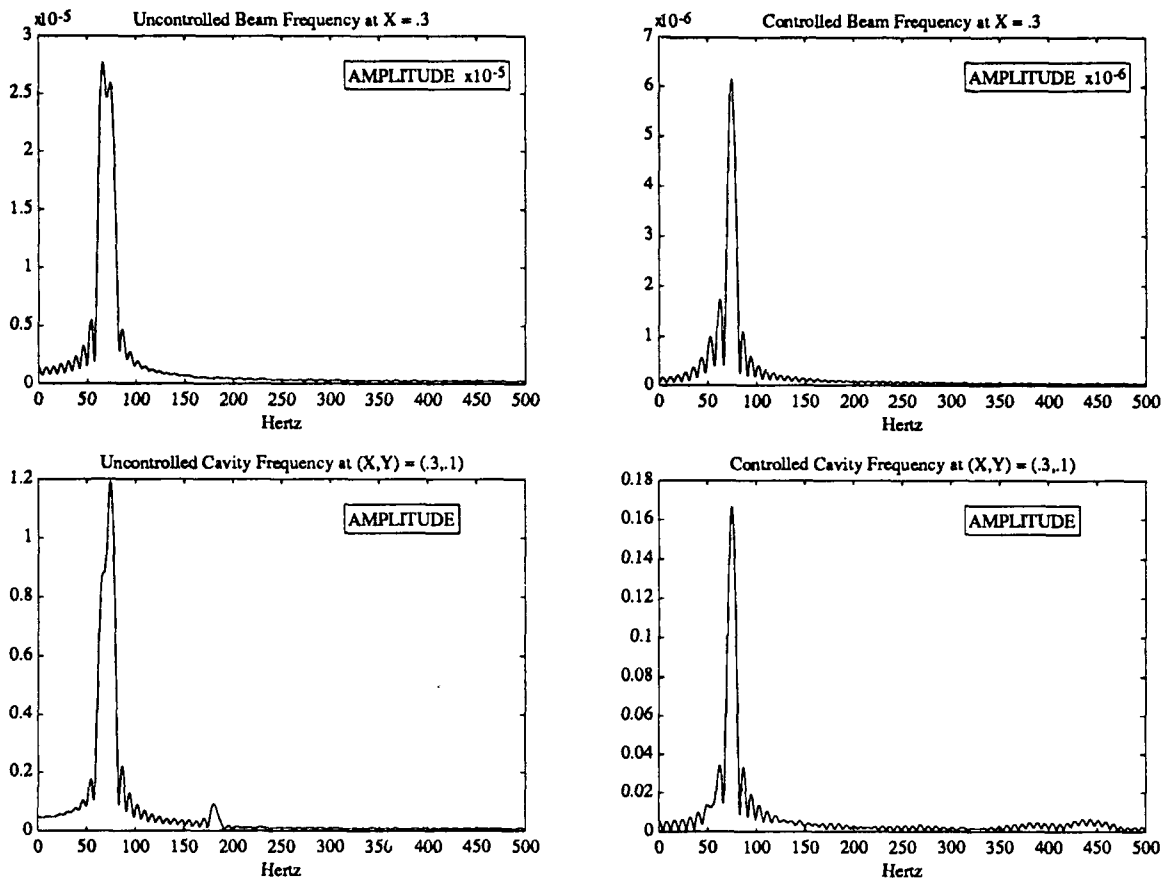


Figure 7. Uncontrolled and controlled beam and cavity frequencies.

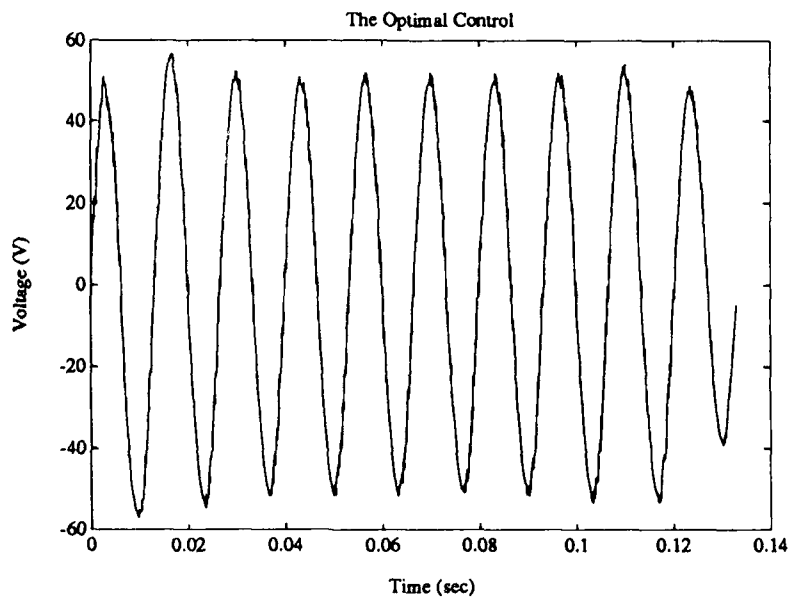


Figure 8. The optimal control  $u(t)$ .

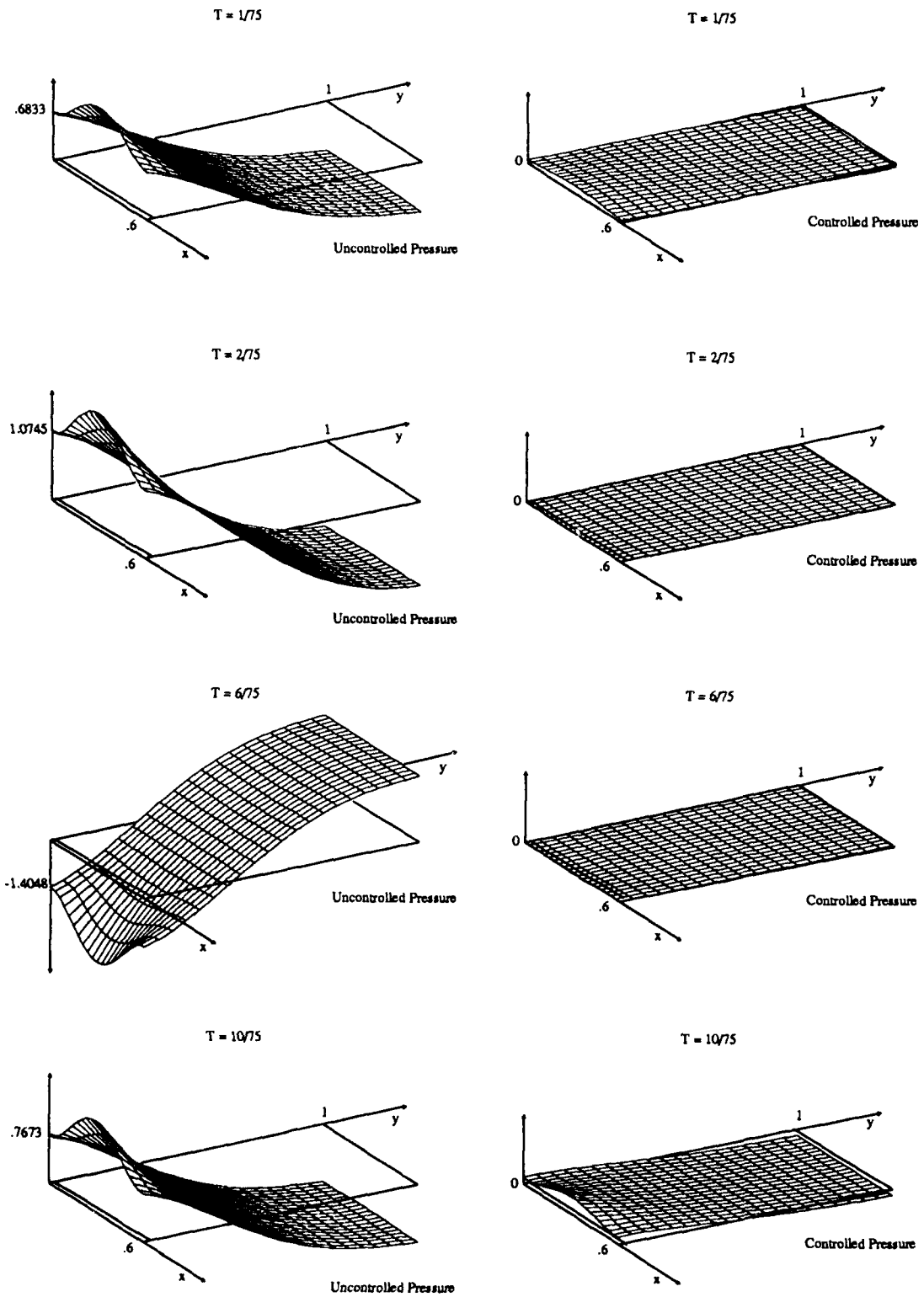


Figure 9. Uncontrolled and controlled pressures.

### 4.3 Multiple Resonant Excitation

The forcing function for this example is

$$f(t, x) = 2.04 [\sin(150\pi t) + \sin(790\pi t)]$$

and hence excites the first and fourth system modes which have natural frequencies of 65.9 and 387.8 hertz, respectively (see Section 4.1). This models a periodic plane wave with a sound pressure level of 120 dB.

Control was again implemented via a single centered piezoceramic patch covering 1/6 of the beam length as shown in Figure 5. The results reported below were obtained with the choices  $d_1 = d_2 = d_4 = 1$ ,  $d_3 = 10^4$  and  $R = 10^{-6}$  for the quadratic cost functional parameters. Several other combinations were tried but these reported values provided a good balance between the amount of pressure reduction obtained and the amount of controlling voltage applied to the piezoceramic patches.

From numerical tests, it was found that the uncontrolled and controlled beam and pressure oscillations could be resolved with the choices  $m_x = m_y = 10$  and  $n = 16$  and the following results were obtained with these values. The need for a larger number of basis functions than were used in Section 4.2 reflects the presence of higher frequency oscillations which resulted from the higher frequency component of the forcing function.

The time interval of interest in this example was taken to be  $[0, 9/75]$  and the uncontrolled beam displacements and acoustic pressures at the points  $X = .3$  and  $(X, Y) = (.3, .1)$  are plotted in Figures 10 and 14. Control was implemented at time  $T = 0$  to obtain the controlled solution plots in Figure 10 while the corresponding plots in Figure 14 show the results obtained when the system was allowed to run uncontrolled until  $T = 3/75 = .04$  seconds at which point the controlling voltage was applied. The frequency plots in Figure 11 correspond to the results in Figure 10. The primary frequencies in both the uncontrolled and controlled problems are the driving frequencies of 75 and 395 hertz. In the uncontrolled case, there is also a low energy system response at 519.5 hertz (recall that the third harmonic in the  $y$ -direction for the uncoupled cavity is at 514 hertz). By comparing the scales in the plots of Figure 11, one can see that the energy in the controlled frequency responses is approximately one tenth of that found in the uncontrolled responses.

From Figure 10, it is seen that when control is started at  $T = 0$ , the solutions are periodic and are maintained at a level which is about 12% of that found in the uncontrolled case. By calculating the root mean square pressures, it was determined that at the point  $(X, Y) = (.3, .1)$ , the uncontrolled sound pressure level is 97.75 dB whereas the controlled sound pressure in this case is maintained at a level of 78.93 dB. The two dimensional surface plots in Figure 13 show spatial slices of the uncontrolled and controlled pressures at the times  $T = 1/75, 3/75, 5/75$  and  $9/75$  for the case when control was started at  $T = 0$ . These plots in conjunction with those in Figure 10 show that even in the case of strong multiple frequency input, the pressure and beam displacement are uniformly reduced and maintained at a very low level throughout the time period. They also demonstrate that the small near field acoustic response which remains near the beam quickly decays as one moves further into the cavity.

The controlling voltage  $u(t)$  obtained with control starting at  $T = 0$  is plotted in Figure 12. As in Section 4.2, it is periodic although in this case, it also reflects the high

frequency contributions of the forcing function. The magnitude remains below 70V which again, is a physically reasonable voltage to apply into the piezoceramic patch. We remark that this voltage can be decreased without any loss of control by using longer centered patches.

As seen in Figure 14, the implementation of control at  $T = 3/75 = .04$  seconds implies that the control scheme is starting with an initial beam displacement of  $-2.4 \times 10^{-5} m$  at  $X = .3$  and an initial pressure of  $1.8 N/m^2$  at  $(X, Y) = (.3, .1)$ . By  $T = .06$  however, both the beam displacement and pressure have been reduced to the levels obtained when the controlling voltage was applied at  $T = 0$  (see Figure 10), and the solutions are maintained at this level throughout the rest of the time interval. The controlling voltage  $u(t)$  for this case is plotted in Figure 15. As expected, it is quite large when the control is initially applied but quickly decreases and is periodic with magnitude less than 70V throughout the second half of the time interval. The magnitude of the controlling voltage can again be reduced by using longer centered patches. These results demonstrate that this methodology is useful not only for maintaining a low level of pressure oscillations throughout the time interval, but also for reducing pressure oscillations which have been allowed to build up in the cavity.

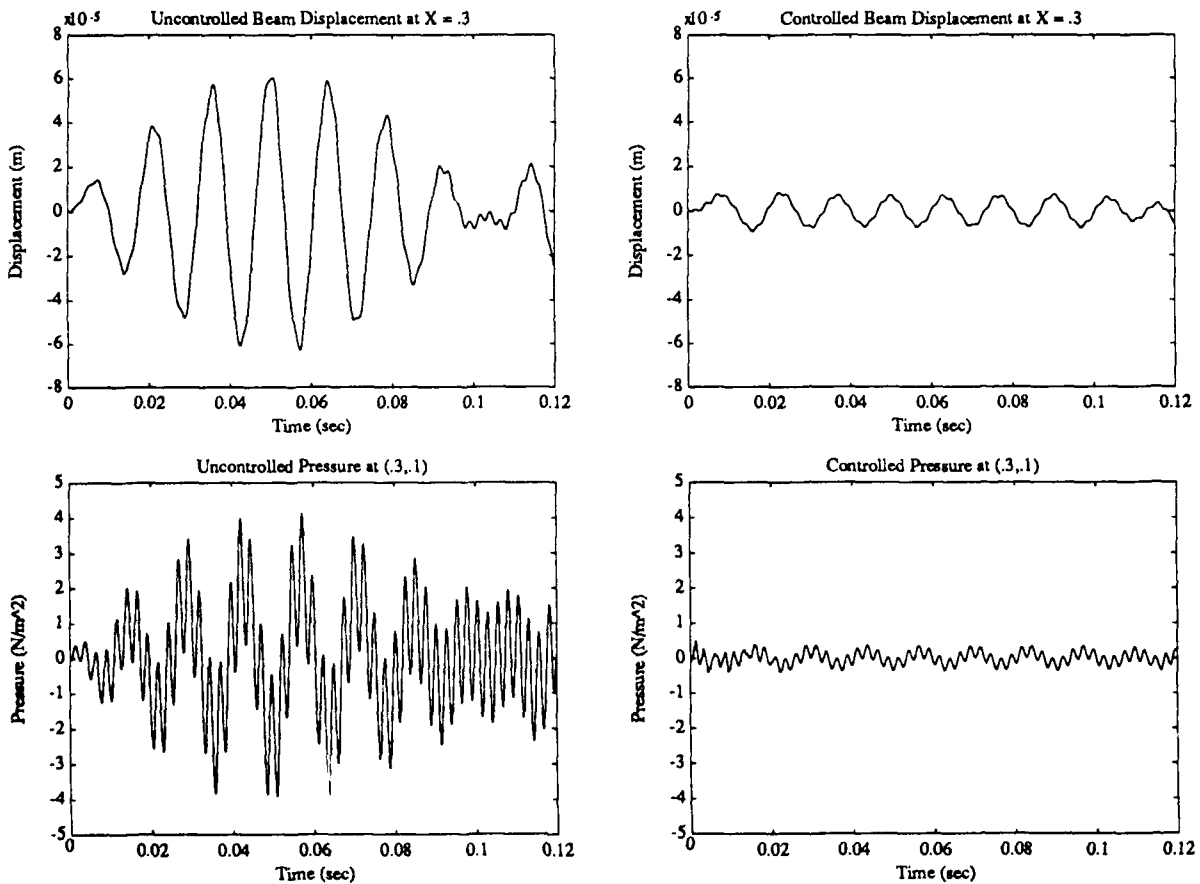


**Figure 10.** Uncontrolled and controlled beam displacements and pressures at the points  $X = .3$  and  $(X, Y) = (.3, .1)$ . Control is started at  $T = 0$ .

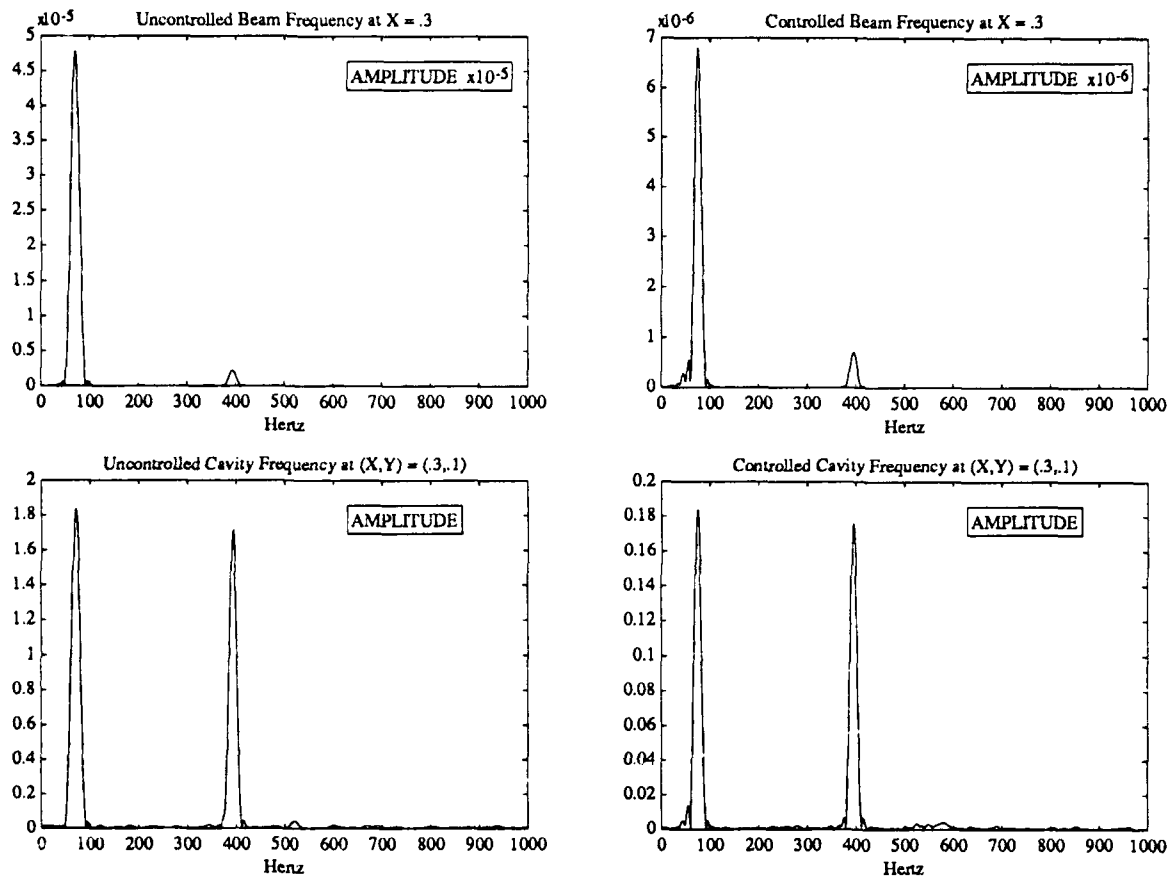


Figure 11. Uncontrolled and controlled beam and cavity frequencies when control is started at  $T = 0$ .

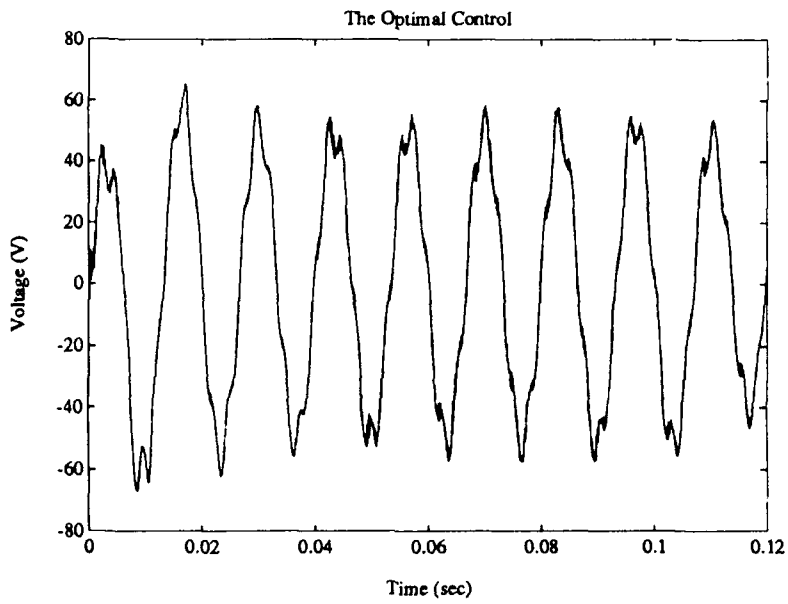


Figure 12. The optimal control  $u(t)$  when control is started at  $T = 0$ .

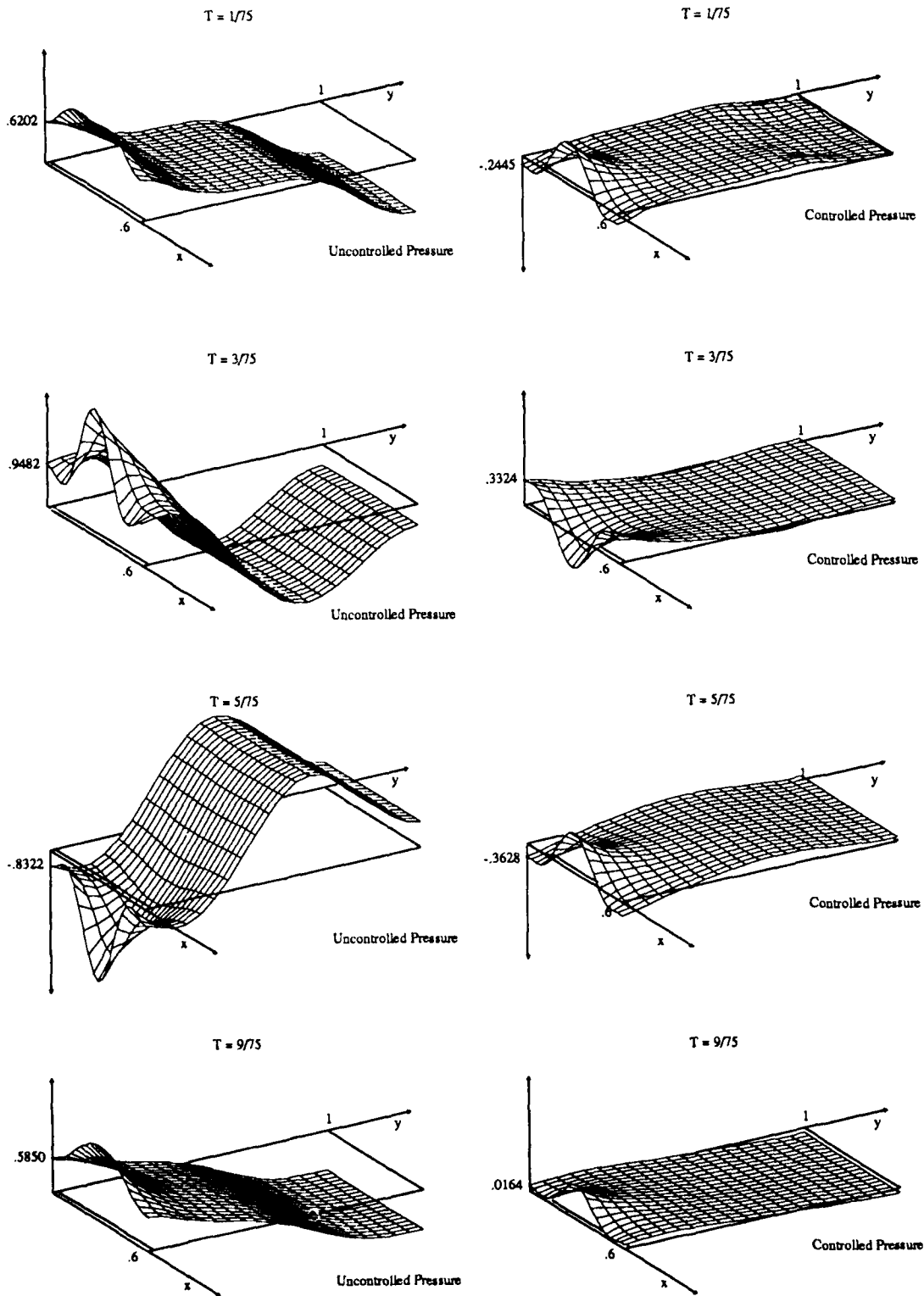
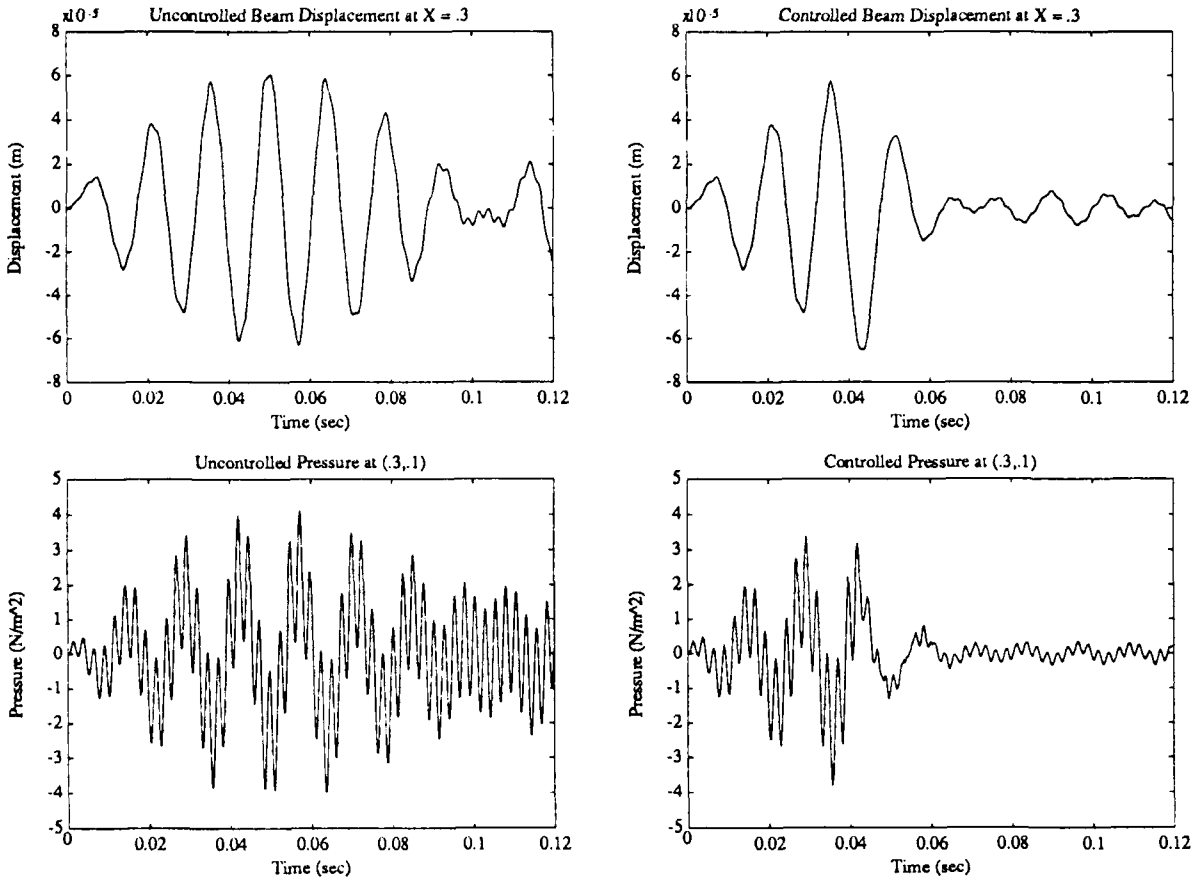
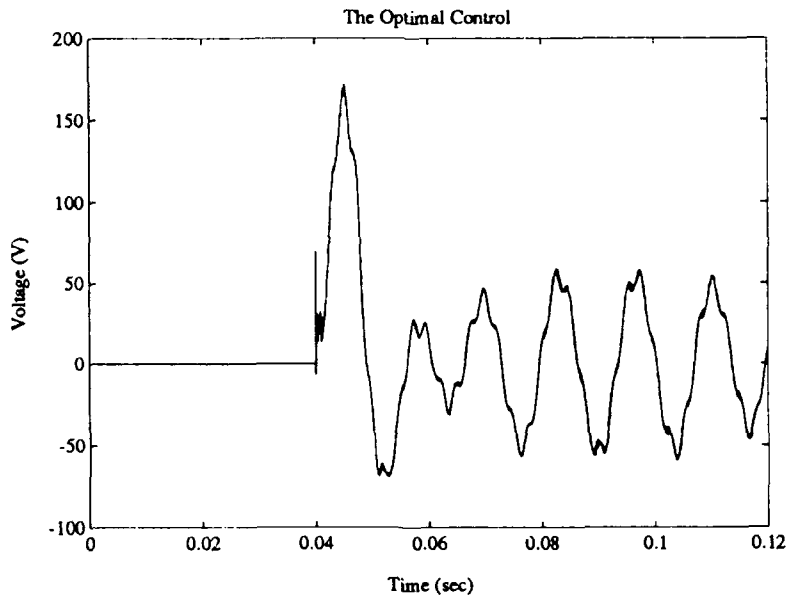


Figure 13. Uncontrolled and controlled pressures when control is started at  $T = 0$ .



**Figure 14.** Uncontrolled and controlled beam displacements and pressures at the points  $X = .3$  and  $(X, Y) = (.3, .1)$ . Control is started at  $T = 3/75 = .04$  seconds.



**Figure 15.** The optimal control  $u(t)$  when control is started at  $T = 3/75 = .04$  seconds.

#### 4.4 Off-Resonant Excitation

In this example, the forcing function was taken to be

$$f(t, x) = 2.04 \sin(470\pi t)$$

with a frequency of 235 hertz which is half way between the natural frequencies of the first and fourth system modes. As noted in Section 4.2, this models a periodic plane wave with an rms sound pressure level of 117 dB.

Control in this example was implemented via a single centered piezoceramic patch covering 1/2 of the beam length as shown in Figure 16. As in the previous examples, several combinations of the quadratic cost functional parameters were tried with the choices  $d_1 = d_2 = d_4 = 1$ ,  $d_3 = 10^4$  and  $R = 10^{-6}$  providing a good balance between the amount of controlling voltage applied to the piezoceramic patches and the amount of reduction in pressure fluctuations which could be obtained. Multiple patches of shorter length were also tried but it was found that for the symmetric forcing function being applied, the single patch provided the best control.

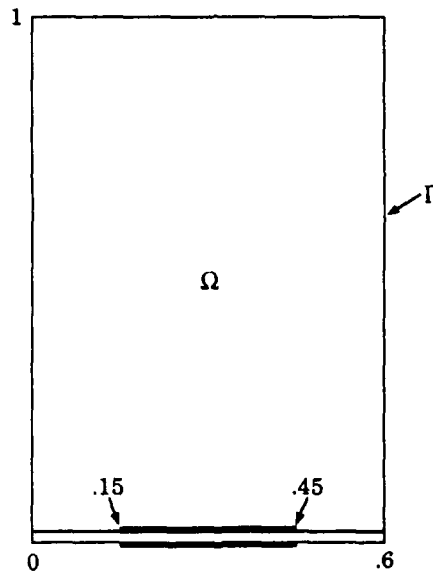


**Figure 16.** Acoustic chamber with one centered 1/2 length piezoceramic patch.

From numerical tests, it was determined that the uncontrolled solutions could be resolved with  $m_x = m_y = 8$ ,  $n = 12$  basis functions whereas  $m_x = m_y = 12$ ,  $n = 16$  were needed to resolve the controlled beam and pressure oscillations due to the transient high frequency responses to the controlling voltage. The results below were obtained with these discretization sizes.

From Figure 18, it can be seen that the uncontrolled responses exhibit not only the driving frequency but also transient excitations at 65.9, 181.6, 345.2, 387.7 and 519.5 hertz which are due to the natural frequencies of the coupled system. The presence of the multiple frequencies can also be seen in the plots of the uncontrolled beam displacement and pressure which are given in Figure 17. The time interval in both cases was taken to be  $[0, 16/235]$ .

The control plots in Figure 17 demonstrate that after a transient phase of about three periods, both the beam displacement and pressure are significantly reduced and maintained at a low magnitude throughout the rest of the time interval. At the point  $(X, Y) = (.3, .1)$ , the uncontrolled sound pressure level is 82.8 dB whereas the controlled sound pressure level is reduced 15.7 dB to 67.1 dB. The frequency plots of the controlled solutions (see Figure 18) show that the dominant response is the driving frequency of 235 hertz. These plots also indicate the presence of a higher frequency response to the control at 519.5 hertz which is much more significant than in the uncontrolled case. This response is transient however, and results taken further out in time indicate that by approximately 48 periods, it is gone. We have also found that when longer patches are used (for example,  $2/3$  length patches), the transient high frequency response is much smaller than that observed here.

To further illustrate the state reduction with feedback control via the piezoceramic patches, the uncontrolled and controlled acoustic pressures at the times  $T = 1/235$ ,  $T = 3/235$ ,  $T = 10/235$  and  $T = 16/235$  are plotted in Figure 20. These results reinforce those in shown in Figure 17 which show that after a transient phase in which the controlled pressure undergoes high frequency, low magnitude oscillations, the pressure field settles into the frequency of the driving force and is uniformly maintained at a low level throughout the time interval.

Figure 19 contains a plot of the controlling voltage,  $u(t)$ . It too is periodic and remains at a magnitude of less than 25 volts.

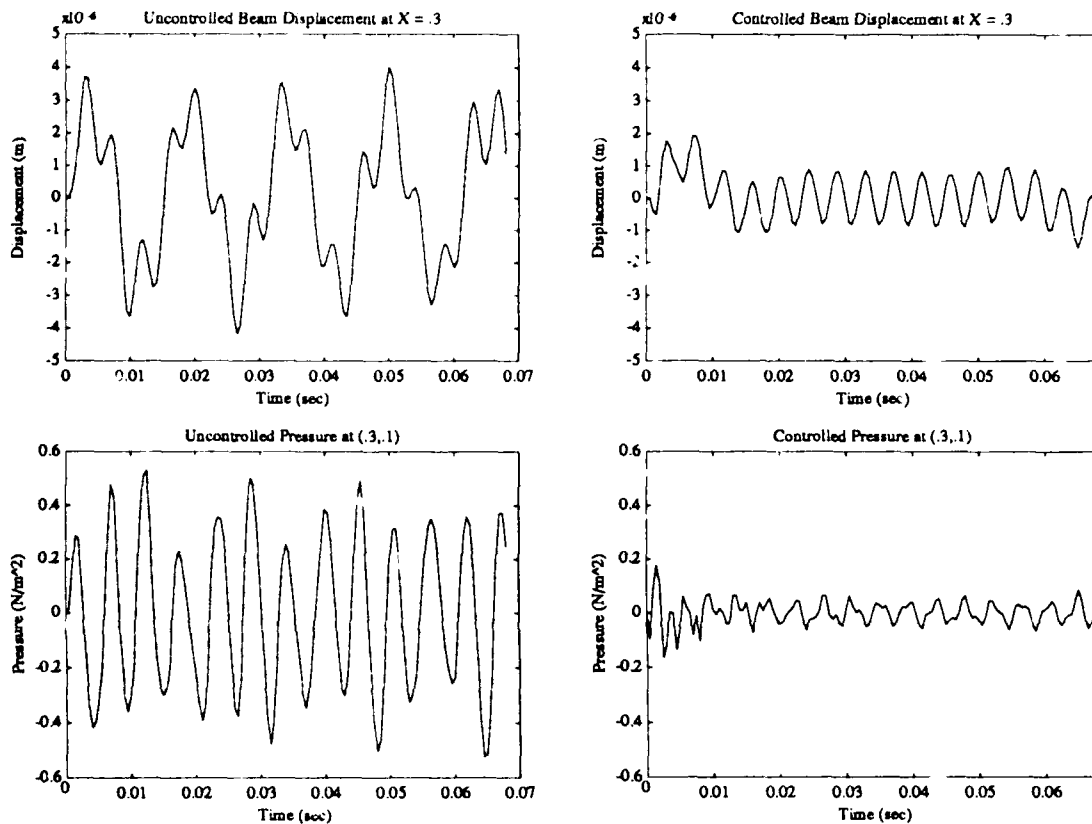


**Figure 17.** Uncontrolled and controlled beam displacements and pressures at the points  $X = .3$  and  $(X, Y) = (.3, .1)$  throughout the time interval  $[0, 16/235]$ .

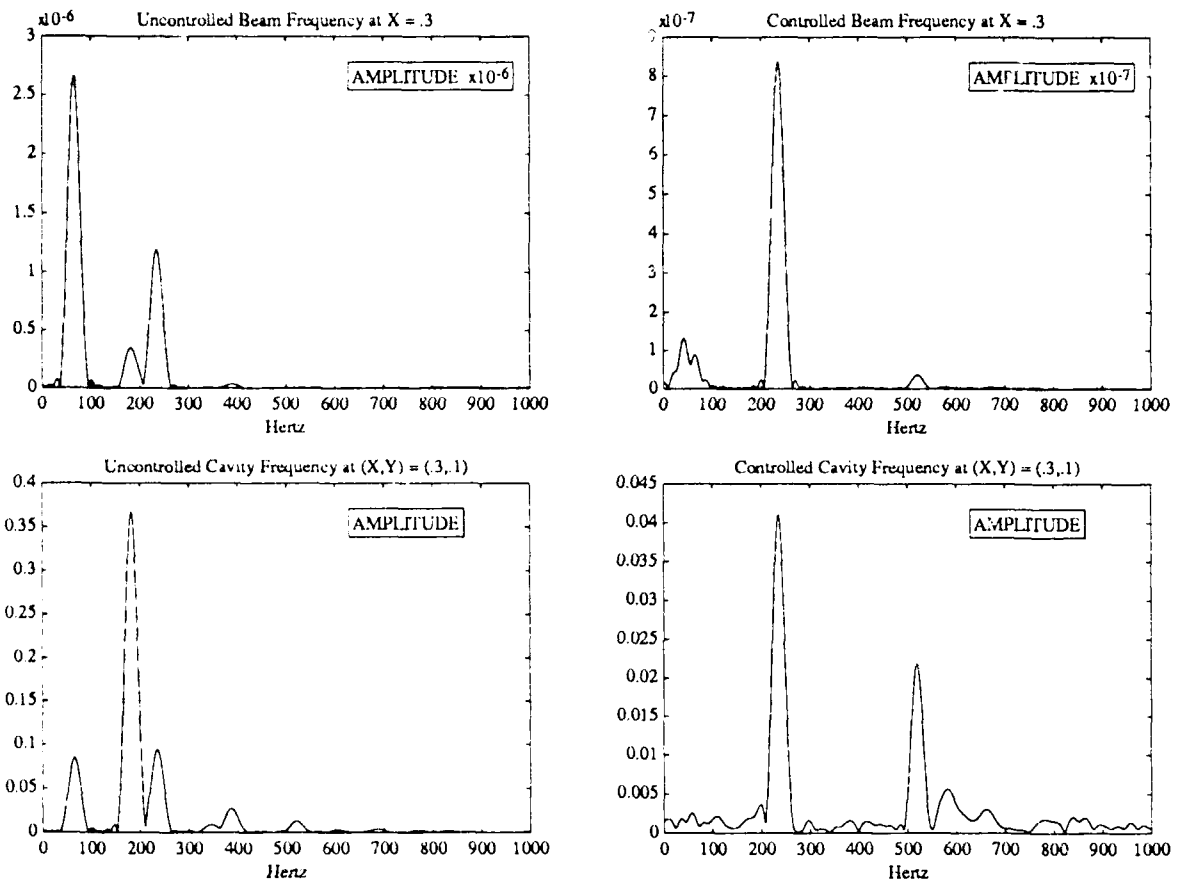


Figure 18. Uncontrolled and controlled beam and cavity frequencies.

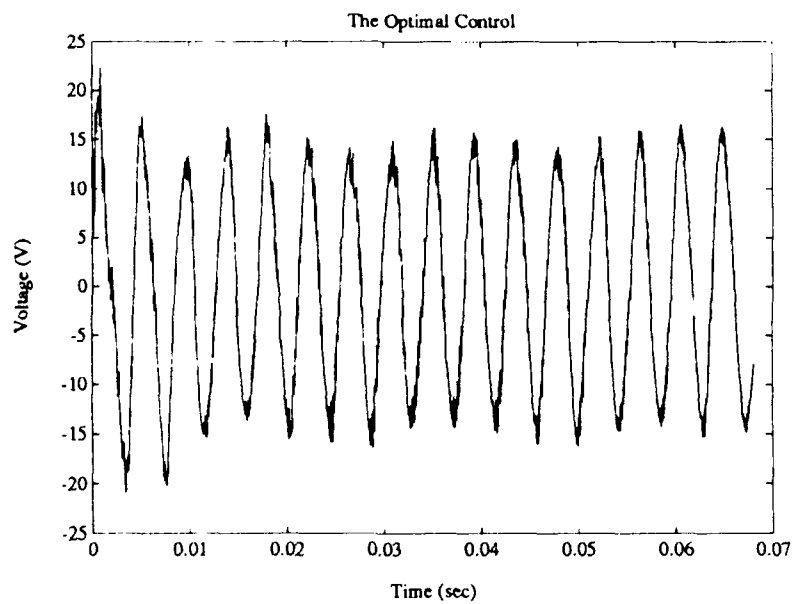


Figure 19. The optimal control  $u(t)$ .

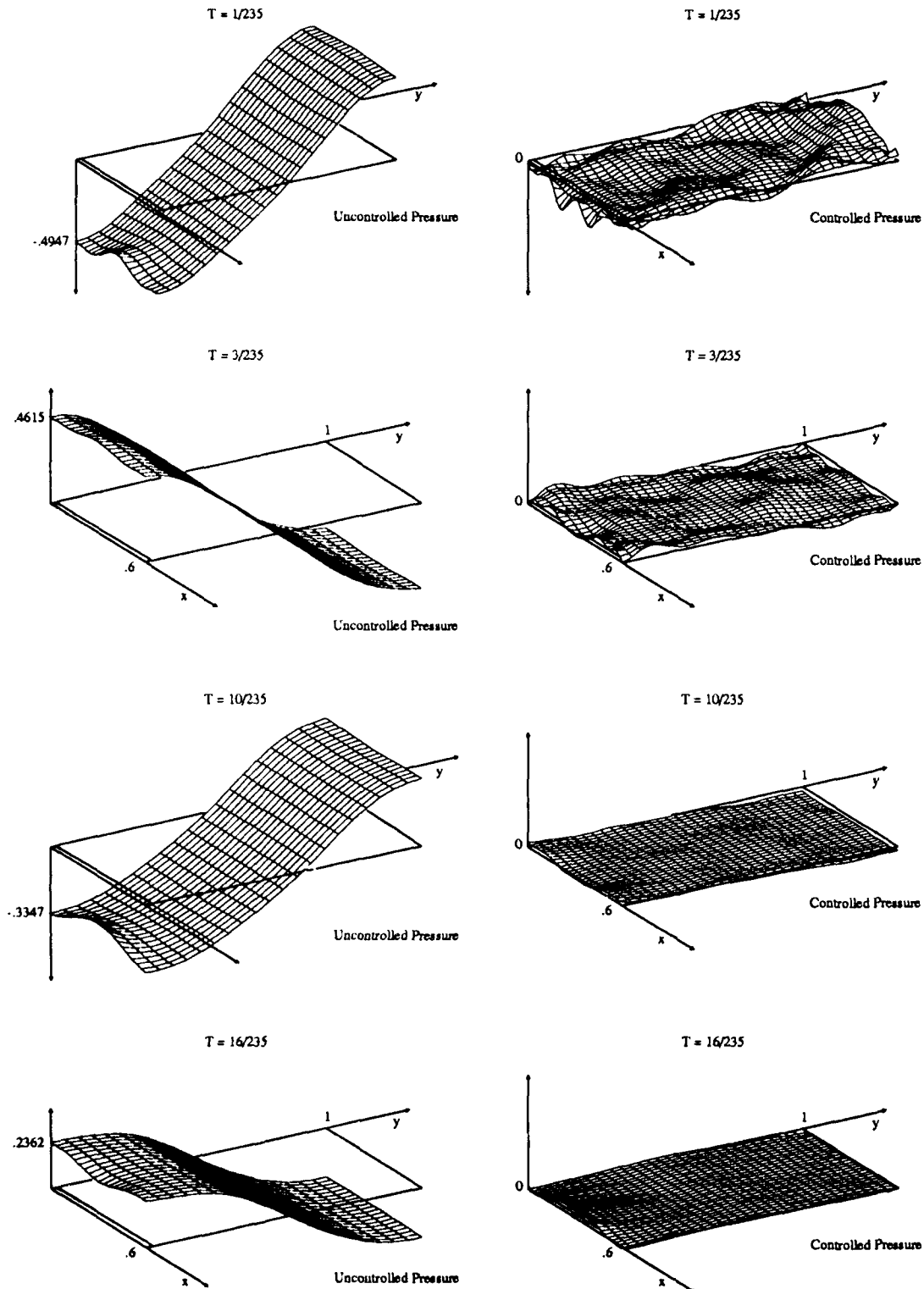


Figure 20. Uncontrolled and controlled pressures.

## 5 Conclusion

In this work we continued the study of active noise control techniques for 2-D structural acoustics problems. The example which we considered consists of a 2-D interior cavity with an active beam at one end. A perturbing force due to an exterior noise source is placed on the beam thus causing fluctuations in the interior acoustic pressure field and hence unwanted noise. Control is implemented in the model via piezoceramic patches on the beam which are excited in a manner so as to produce pure bending moments. Approximation techniques are discussed and by writing the resulting system as an abstract Cauchy equation, the problem of reducing interior pressure fluctuations can be posed in the context of an LQR time domain state space formulation.

Several examples are considered which demonstrate both modeling and control results. The first example illustrates the dynamic behavior of the coupled system. By looking at the natural frequencies, it can be seen that although many of the features of the uncoupled and undamped beam and cavity are present, some variations occur in the system of interest since it involves not only coupling between the cavity and beam equations but also includes damping in the beam.

In the rest of the examples, harmonic forcing functions of various frequencies but modeling a uniform pressure excitation are applied to the beam, and results demonstrating the reduction of interior cavity pressure and beam displacement under feedback control are presented. Although the forcing functions were chosen to strongly excite various system frequencies, the results show that input of the optimally controlling voltage  $u(t)$  uniformly reduces both the pressure and the beam displacement and maintains them at a very low level of magnitude throughout the time intervals of interest. Moreover, as indicated by the results of Section 4.3, this methodology is useful not only for maintaining a low level of pressure oscillations throughout the time interval, but also for reducing pressure oscillations which have been allowed to build up in the cavity.

Numerical results have indicated that for a 1-D uniform periodic forcing function, the best results can be obtained with one centered patch with the amount of control increasing with increasing patch length. By increasing the length of the patch, one can also, in many cases, decrease the amount of voltage needed to reduce interior pressure oscillations. In the examples that we have considered however, the magnitude of the controlling voltage has always remained in a range which is physically reasonable to apply to the piezoceramic patches.

**ACKNOWLEDGEMENT:** The authors would like to express their sincere appreciation to H.C. Lester of the Acoustics Division, NASA Langley Research Center, for input during numerous discussions concerning the modeling of the acoustic problem.

## References

- [1] H.T. Banks, W. Fang, R.J. Silcox and R.C. Smith, Approximation methods for control of acoustic/structure models with piezoceramic actuators, Submitted to J. Intelligent Material Systems and Structures.
- [2] H.T. Banks and K. Ito, A unified framework for approximation in inverse problems for distributed parameter systems, *Control-Theory and Advanced Technology*, 4 (1988), 73-90.
- [3] H.T. Banks and K. Ito, Approximation in LQR problems for infinite dimensional systems with unbounded input operators, *Proc. Conf. on Optimization*, Haifa, 1992, to appear.
- [4] H.T. Banks, S.L. Keeling, and R.J. Silcox, Optimal control techniques for active noise suppression, *Proc. 27th IEEE Conf. on Decision and Control*, Austin, Texas, 1988, 2006-2011.
- [5] H.T. Banks, S.L. Keeling, and C. Wang, Linear quadratic tracking problems in infinite dimensional Hilbert spaces and a finite dimensional approximation framework, LCDC/CCS Rep. 88-28, October, 1988, Brown University.
- [6] R.L. Clark, Jr., C.R. Fuller and A. Wicks, Characterization of multiple piezoelectric actuators for structural excitation, *J. Acoust. Soc. Amer.*, 1992, to appear.
- [7] E.F. Crawley and E.H. Anderson, Detailed models of piezoceramic actuation of beams, *AIAA Conf. Paper 89-1388-CP*, 1989, 2000-2010.
- [8] G. Da Prato, Synthesis of optimal control for an infinite dimensional periodic problem, *SIAM J. Control Opt.*, 25 (1987), 706-714.
- [9] E.K. Dimitriadis, C.R. Fuller and C.A. Rogers, Piezoelectric actuators for distributed noise and vibration excitation of thin plates, *Proc. 8th ASME Conf. on Failure, Prevention, Reliability and Stress Analysis*, Montreal, 1989, 223-233.
- [10] F. Fakhroo, Legendre-Tau approximation for an active noise control problem, Ph.D. Thesis, May, 1991, Brown University, Providence, RI.
- [11] C.R. Fuller, C.A. Rogers and H.H. Robertshaw, Active structural acoustic control with smart structures, *SPIE Conference 1170 on Fiber Optic Smart Structures and Skins II*, Boston, MA 1989.
- [12] C.R. Fuller, S.D. Snyder, C.H. Hansen and R.J. Silcox, Active control of interior noise in model aircraft fuselages using piezoceramic actuators, *AIAA Thirteenth Aeroacoustics Conference*, Tallahassee, FL 1990.
- [13] H.C. Lester and C.R. Fuller, Active control of propeller induced noise fields inside a flexible cylinder, *AIAA Tenth Aeroacoustics Conference*, Seattle, WA, 1986.

- [14] I. Malecki, *Physical Foundations of Technical Acoustics*, Translated by I. Bellert, Pergamon Press, New York, 1969.
- [15] P.M. Morse and K.U. Ingard, *Theoretical Acoustics*, McGraw-Hill, New York, 1968.
- [16] J. Pan and C.H. Hansen, Active control of noise transmission through a panel into a cavity. II: Experimental Study, *J. Acoust. Soc. Am.*, **90** (3), (1991), 1488-1492.
- [17] J. Pan and C.H. Hansen, Active control of noise transmission through a panel into a cavity. III: Effect of the actuator location, *J. Acoust. Soc. Am.*, **90** (3), (1991), 1493-1501.
- [18] J.E. Potter, Matrix quadratic solutions, *SIAM J. Appl. Math.*, **14** (1966), 496-501.
- [19] R.J. Silcox, S. Lefebvre, V.L. Metcalf, T.B. Beyer and C.R. Fuller, Evaluation of piezoceramic actuators for control of aircraft interior noise, *Proc. of the DGLR/AIAA 14th Aeroacoustics Conf.*, Aachen, Germany, May 11-14, 1992.

# REPORT DOCUMENTATION PAGE

Form Approved  
OMB No. 0704-0188

Public reporting burden for this collection of information is estimated to average 1 hour per response, including the time for reviewing instructions, searching existing data sources, gathering and maintaining the data needed, and completing and reviewing the collection of information. Send comments regarding this burden estimate or any other aspect of this collection of information, including suggestions for reducing this burden, to Washington Headquarters Services, Directorate for Information Operations and Reports, 1215 Jefferson Davis Highway, Suite 1204, Arlington, VA 22202-4302, and to the Office of Management and Budget, Paperwork Reduction Project (0704-0188), Washington, DC 20503.

<b>1. AGENCY USE ONLY (Leave blank)</b>		<b>2. REPORT DATE</b> April 1992	<b>3. REPORT TYPE AND DATES COVERED</b> Contractor Report	
<b>4. TITLE AND SUBTITLE</b> THE MODELING AND CONTROL OF ACOUSTIC/STRUCTURE INTERACTION PROBLEMS VIA PIEZOCERAMIC ACTUATORS: 2-D NUMERICAL EXAMPLES			<b>5. FUNDING NUMBERS</b> C NAS1-18605  WU 505-90-52-01	
<b>6. AUTHOR(S)</b> H. T. Banks R. J. Silcox R. C. Smith				
<b>7. PERFORMING ORGANIZATION NAME(S) AND ADDRESS(ES)</b> Institute for Computer Applications in Science and Engineering Mail Stop 132C, NASA Langley Research Center Hampton, VA 23665-5225			<b>8. PERFORMING ORGANIZATION REPORT NUMBER</b>  ICASE Report No. 92-17	
<b>9. SPONSORING/MONITORING AGENCY NAME(S) AND ADDRESS(ES)</b> National Aeronautics and Space Administration Langley Research Center Hampton, VA 23665-5225			<b>10. SPONSORING/MONITORING AGENCY REPORT NUMBER</b>  NASA CR-189639 ICASE Report No. 92-17	
<b>11. SUPPLEMENTARY NOTES</b> Langley Technical Monitor: Michael F. Card Final Report				
			Submitted to Proc. for the ASME 1992 Winter Annual Meeting Symposium on Active Control of Noise and Vibration	
<b>12a. DISTRIBUTION/AVAILABILITY STATEMENT</b> Unclassified - Unlimited  Subject Category 64, 66			<b>12b. DISTRIBUTION CODE</b>	
<b>13. ABSTRACT (Maximum 200 words)</b> The modeling and active control of acoustic pressure in a 2-D cavity with a flexible boundary (a beam) is considered. Control is implemented in the model via piezoceramic patches on the beam which are excited in a manner so as to produce pure bending moments. The incorporation of the feedback control in this manner leads to a system with an unbounded input term. Approximation techniques are discussed and by writing the resulting system as an abstract Cauchy equation, the problem of reducing interior pressure fluctuations can be posed in the context of an LQR time domain state space formulation. Examples illustrating the dynamic behavior of the coupled system as well as demonstrating the viability of the control method on a variety of problems with periodic forcing functions are presented.				
<b>14. SUBJECT TERMS</b>  feedback control in structural acoustics models; piezoceramic actuators; LQR state space formulation			<b>15. NUMBER OF PAGES</b> 30	
			<b>16. PRICE CODE</b> A03	
<b>17. SECURITY CLASSIFICATION OF REPORT</b> Unclassified	<b>18. SECURITY CLASSIFICATION OF THIS PAGE</b> Unclassified	<b>19. SECURITY CLASSIFICATION OF ABSTRACT</b>	<b>20. LIMITATION OF ABSTRACT</b>	

NSN 7540-01-280-5500

Standard Form 298 (Rev. 2-89)  
Prescribed by ANSI Std. Z39-18  
298-102